ACS SyntheticBiology

pubs.acs.org/synthbio Research Article

Downhill (Un)Folding Coupled to Binding as a Mechanism for Engineering Broadband Protein Conformational Transducers

Suhani Nagpal,[#] Thinh D. N. Luong,[#] Mourad Sadqi, and Victor Muñoz*

Cite This: *ACS Synth. Biol.* 2020, 9, 2427–2439 Read Online

ACCESS | Metrics & More | Article Recommendations | Supporting Information

ABSTRACT: Canonical proteins fold and function as conformational switches that toggle between their folded (on) and unfolded (off) states, a mechanism that also provides the basis for engineering transducers for biosensor applications. One of the limitations of such transducers, however, is their relatively narrow operational range, limited to ligand concentrations 20-fold below or above their C_{50}. Previously, we discovered that certain fast-folding proteins lose/gain structure gradually (downhill folding), which led us to postulate their operation as conformational rheostats capable of processing inputs/outputs in analog fashion. Conformational rheostats could make transducers with extended sensitivity. Here we investigate this hypothesis by engineering pH transducing into the naturally pH insensitive, downhill folding protein gpW. Particularly, we engineered histidine grafts into its hydrophobic core to induce unfolding *via* histidine ionization. We designed and tested the effects of ionization *via* computational modeling and studied experimentally the four most promising single grafts and two double grafts. All tested mutants become reversible pH transducers in the 4−9 range, and their response increases proportionally to how buried the histidine graft is. Importantly, the pH-dependent reversible (un)folding occurs in rheostatic fashion, so the engineered transducers can detect up to 6 orders of magnitude in $[H^+]$ for single grafts, and even more for double grafts. Our results demonstrate that downhill (un)folding coupled to binding produces the gradual, analog responses to the ligand (here H^+) that are expected of conformational rheostats, and which make them a powerful mechanism for engineering transducers with sensitivity over many orders of magnitude in ligand concentration (broadband).

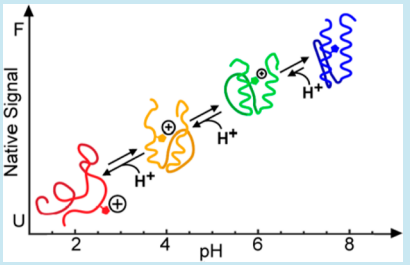

The engineering of protein folding/unfolding equilibria coupled to binding to a suitable ligand offers a generalizable strategy for developing biosensors that exploits the unparalleled specificity and selectivity of protein-mediated biomolecular recognition.[1] The strategy entails engineering the protein to be intrinsically unstable in the absence of ligand and use the free energy provided by binding to the analyte in question (which only binds to the native structure) to trigger refolding, thus transducing the binding event into a monitorable output.[2] These transducers toggle between the unfolded-free and the folded-bound states given that their folding mechanism is usually two-state and the native structure is only formed upon binding the ligand, thus exemplifying the operation of conformational switches.[3] The results are binary signals and typically sigmoidal saturation curves that provide sensitivity to ligand concentrations within 20-fold below and above the apparent K_d or C_{50}.[4] Another characteristic of such transducers is that their time response is ultimately determined by the rate of folding into their native state, which can take up to minutes for two-state folding proteins.[5] These characteristics make it challenging to produce protein transducers capable of broadband and/or real-time sensing, features that are often desired in biosensing applications.

In that regard, one exciting possibility is to use downhill folding proteins as scaffolds for building transducers based on (un)folding coupled to binding. Downhill proteins fold and unfold in very short times (microseconds),[6] and change their structural properties gradually upon (de)stabilization,[7] which results in broad, structurally heterogeneous (un)folding transitions.[8,9] In fact, it has been proposed that the thermodynamic coupling between a biological signal and the gradual (un)folding of a downhill protein can result in conformational rheostats, a mechanism by which the protein produces analog responses to the input strength, *e.g.*, ligand concentration.[10] The noncanonical features of downhill protein folding present a unique opportunity for building conformational transducers with broadband sensitivity and real time response. Initially, we explored the merit of this idea on the BBL domain, a showcase of the most extreme, one-state downhill (un)folding behavior[7] and microsecond folding kinetics.[11] BBL folding is naturally pH sensitive due to two histidine residues that are partially buried within the protein core. A detailed study of the pH response of BBL has shown that this protein changes its structure gradually over 4 orders of

Received: April 7, 2020
Published: August 21, 2020

https://dx.doi.org/10.1021/acssynbio.0c00190
ACS Synth. Biol. 2020, 9, 2427−2439

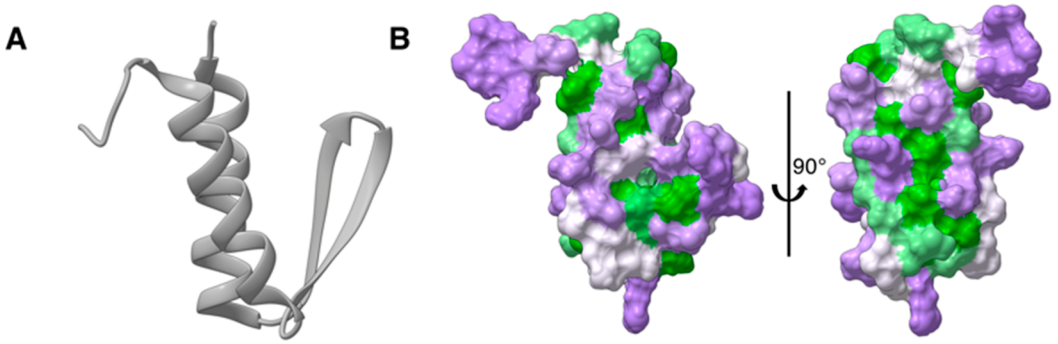

Figure 1. Structural features of gpW. (A) The protein is composed of 62 residues forming an all-antiparallel $\alpha + \beta$ topology consisting of one β-hairpin and two α-helices. (B) Molecular surface representation of the gpW native structure with color coding signifying the degree of hydrophobicity from polar (purple), intermediate (white), to hydrophobic (green). The two projections highlight the cores between helix-2 and the β-hairpin (left) and between the two helices (right).

magnitude in proton concentration and can record changes in pH with response times of a few microseconds.[12]

The BBL study did not address the issue of whether such remarkable broadband response is extensible to other downhill (un)folding coupled to binding processes, or rather a unique result of natural selection on BBL. To determine the extensibility of the broadband response of transducers based on downhill (un)folding coupled to binding, and rationalize its structural/energetic determinants, we decided to *de novo* engineer pH transducing into gpW (W protein of bacteriophage lambda). GpW is a protein that folds into an $\alpha+\beta$ topology[13] and is stable and unaffected by pH in the 4−9 range.[14] Moreover, gpW folds and unfolds in microseconds, and exhibits the thermodynamic features of a downhill folding domain, including a minimally cooperative unfolding transition and multiprobe dependence,[15] as well as an atomically heterogeneous thermal unfolding process as probed both by NMR and long-time-scale molecular dynamics (MD) simulations.[14] Relative to BBL, gpW is considerably larger (62 *vs* 45 residues), is a full gene product rather than an excised domain,[15] and features an all-antiparallel fold with two distinct hydrophobic cores (Figure 1) that offers various structural loci for engineering pH transducing.

To *de novo* engineer pH transducing into gpW we resorted to a histidine grafting strategy by which we introduce histidine residues into structurally targeted protein locations. Several groups have reported that the dual aromatic/ionic character of histidine and its pK_a value close to physiological pH (*i.e.*, 6−6.5) can induce pH-dependent conformational changes in the native ensemble of a variety of proteins.[16−21] The role of histidine ionization as trigger of conformational transitions on proteins is also exploited functionally by nature, like in the transmembrane protein OmpG, which opens and closes its central pore in response to the (de)ionization of two histidine residues.[22] The molecular mechanism behind these conformational changes hinges on the ability of the histidine residue to interact favorably with a surrounding hydrophobic environment in nonionic form, and strongly destabilize the same environment when ionized (*i.e.*, due to charge desolvation). Namely, a histidine that is buried into the core of a protein destabilizes the folded state upon ionization by an amount proportional to its drop in pK_a ($\Delta\Delta G^{UN}_{+0} = 2.3026 \times RT\Delta pK_a$). Mutational analyses have shown that the pK_a shifts of buried histidine residues vary widely, being ultimately determined by the local environment in the native structure, including the degree of burial and the interactions with surrounding residues.[23]

Practically, we implemented a computational/experimental histidine grafting strategy in four steps: (i) identification of structural loci in gpW suitable for accommodating a partially buried histidine graft; (ii) mutation design *in silico*, followed by computational assessment of mutant stability through all-atom MD simulations in explicit solvent; (iii) selection of mutations that do not drastically perturb the stability of the native fold in nonionic form, and production in the lab; (iv) computational and experimental analysis of the pH response of each select mutation. Our results on four single and two double histidine grafts on gpW show that the approach reliably introduces a pH-dependent unfolding mechanism onto a protein that is naturally pH insensitive in the 4−9 range. Moreover, the structural changes of the mutants can extend for over >6 orders of magnitude in [H^+], demonstrating that downhill (un)-folding coupled to binding is a powerful approach for engineering broadband conformational transducers.

RESULTS AND DISCUSSION

The Protein gpW and pH Sensing as a Model to Engineer Broadband Transducing. There are several reasons for using pH sensing for this study: (1) proton binding-release is a relatively straightforward process to engineer into proteins using histidine grafts; (2) histidine grafting allows for the introduction of multiple proton binding sites onto the protein scaffold as strategy for amplification or modulation of the transducer response; (3) ionization−deionization processes are the fastest reactions in aqueous solution because proton transfer is orders of magnitude faster than conventional diffusion-controlled processes.[24] Such an ultrafast binding process makes the transducer response time to be solely determined by the conformational transition of the protein, which takes place in microseconds for downhill folders.[25] GpW does indeed fold and unfold in microseconds,[15] but to be a suitable scaffold for this study it also needs to be naturally insensitive to pH in the neutral to mildly acidic range that is most biologically relevant (between 4 and 9). From an amino acid composition viewpoint, gpW has a sole histidine (H15) that is located on the exterior of helix-1 and fully solvent exposed, and therefore unlikely to experience significant pK_a shifts.

We determined the natural pH sensitivity of gpW by measuring the thermal unfolding of the wildtype protein as a function of pH. The results of these experiments are given in

https://dx.doi.org/10.1021/acssynbio.0c00190
ACS Synth. Biol. 2020, 9, 2427−2439

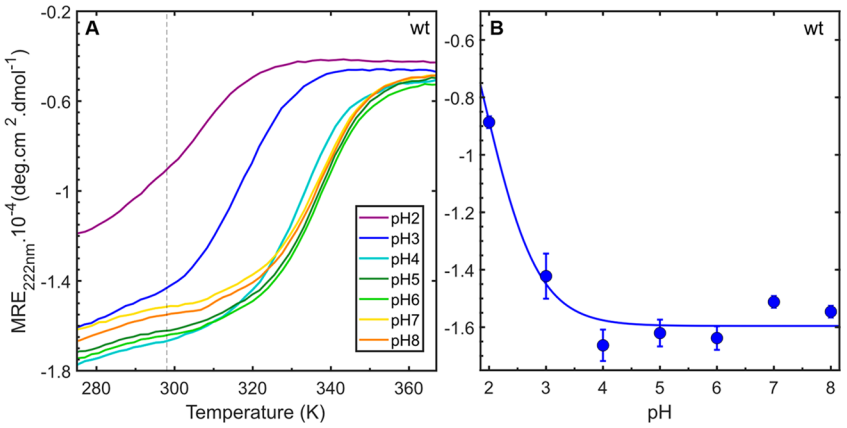

Figure 2. (A) Thermal unfolding curves of gpW at different pH monitoring the changes in the native α-helical content. Each curve is an average of two sets of data. Curves are colored according to the visible light spectrum with the lowest pH corresponding to the highest energy (purple). (B) The blue circles represent the α-helical content of gpW as a function of pH at 298 K. The blue line is to guide the eye.

Figure 2. Panel A shows the thermal unfolding of gpW measured by CD at 222 nm (mean residue ellipticity, $MRE_{222\ nm}$, which reports on the strong native α-helical signal of gpW) as a function of pH. Protein stability appears completely unaffected down to pH 5. At pH 4 there are signs of slight destabilization that is sharply enhanced at lower pH. The behavior of gpW below pH 4 reflects the protonation of its glutamate and aspartate residues, which results in a large positive net charge on the protein (pI > 10) that promotes its unfolding. The destabilization at very low pH is also evident as a drop of the denaturation midpoint temperature (T_m) (Figure S1). However, from the viewpoint of the native signal at room temperature (298 K), the dependence on pH is flat down to pH 4; past this point gpW loses native CD signal, but even at pH 2 there is still about 30% native signal left (Figure 2B). As an additional test, we produced and studied the H15A gpW mutant, which confirmed that removing the imidazole at position 15 does not significantly affect gpW stability as measured by CD, nor its pH sensitivity in the 4−9 range. In other words, gpW emerges as a suitable protein scaffold for engineering conformational pH transducing.

Design Principles of Conformational pH Transducers Based on Histidine Grafting. The imidazole ring of histidine is ionizable with a standard pK_a around 6.5. When the imidazole is deprotonated its aromatic character predominates, and thus it can form stabilizing interactions with neighboring hydrophobic residues within the protein core. On the other hand, a protonated histidine located in a buried position destabilizes the native structure due to the large energetic penalty involved in desolvating the charge. This net destabilization shifts the effective pK_a to lower values (*i.e.*, needing higher proton concentrations to become ionized). The larger the pK_a drop, the stronger the destabilization of the native state that is induced by histidine ionization, which can eventually drive protein unfolding once the destabilization is comparable to the intrinsic stability of the native state.[26] In this regard, as most downhill folding domains,[10] gpW's native state has relatively low intrinsic stability, *i.e.*, about 14 kJ/mol.[15] There are two important implications that emerge from these considerations: (1) histidine grafts should be structurally conservative to avoid excessive destabilization of the gpW scaffold that could result on a protein that is unfolded over the entire pH range; (2) the grafts should still be sufficiently buried (and experience pK_a downshifts) to be able to trigger unfolding upon protonation at mildly acidic pH.

With these principles in mind, we used structural analysis to select the locations on gpW for histidine grafting. The recipient sites are residues that participate in one of the two gpW hydrophobic cores (Figure 1) and have enough space to accommodate the imidazole ring into the cavity without introducing significant steric clashes. We identified six such positions: A10, A13, L7, M18, F35, and V40 (see Methods for more details). The six locations have varying degrees of solvent exposure (Figure S2), hence, providing us with flexibility to engineer different pH responses and explore how to maximize the transducer dynamic range. We then designed the histidine mutations *in silico* and evaluated the effect on the stability of gpW using the DUET algorithm (Table S1). The calculations with DUET indicated that histidine substitutions into the L7, A10, and A13 positions could reduce the native stability of gpW at room temperature by more than half, potentially placing these grafts at the brink of stability even at neutral pH.

Molecular Dynamics Analysis of Histidine Graft Stability. We then used atomistic MD simulations to investigate the intrinsic destabilization induced by the histidine grafts in deprotonated form. Particularly we simulated each of the six mutants and the wildtype for 400 ns. Figure 3 shows the time trajectories of the root-mean-square deviation (RMSD). Given the marginal stability and ultrafast folding of gpW, we expected these relatively short trajectories to display significant structural fluctuations and possibly even global unfolding. The control trajectory on wildtype gpW does show distinct structural transitions that take place within the first 100 ns, followed by stabilization onto a relatively low RMSD ensemble. These fluctuations correspond mostly to the β-hairpin flapping in and out from its interaction with the two helices, which remain closely in contact throughout the simulation. The lower stability and enhanced structural dynamics of the gpW hairpin have been reported before from NMR analysis and long-time scale MD simulations.[14] Simulations of M18H, F35H, and V40H showed minimal structural fluctuations throughout the entire trajectory with RMSD below 0.4 nm throughout (Figure 3A). L7H displays larger structural fluctuations than the other three grafts, and significantly higher mean RMSD (about 0.55 nm), which is consistent with the large destabilization predicted by DUET (Table S1) and its fully buried location in gpW (Figure S2).

https://dx.doi.org/10.1021/acssynbio.0c00190
ACS Synth. Biol. 2020, 9, 2427−2439

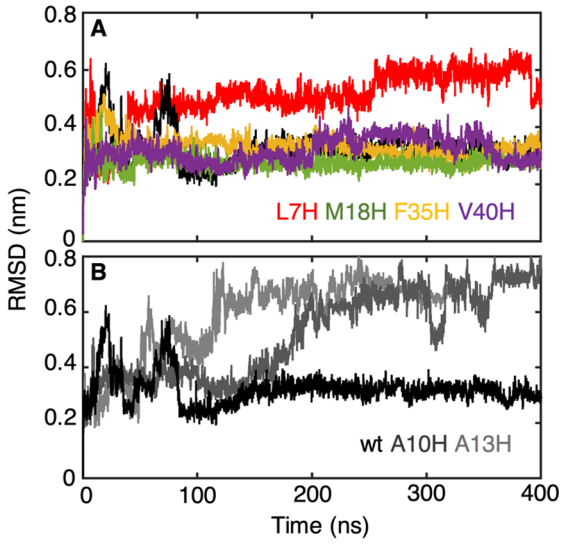

Figure 3. Time evolution of the root-mean-square deviation (RMSD) relative to the lowest energy conformer of the gpW NMR ensemble from MD simulations of gpW (black) and the six designed single (deprotonated) histidine substitutions. (A) Trajectories of the four mutants that show structural fluctuations below the threshold (0.65 nm). (B) Trajectories of the mutants that exceeded the 0.65 nm RMSD threshold.

The structural fluctuations of L7H are more frequent, but they still are comparable in magnitude (≤0.65 nm) to those experienced by the wildtype. Moreover, as in the wildtype, the structural fluctuations of L7H concentrate on the β-hairpin. These results suggest that L7H is probably a viable graft. In contrast, A10H and A13H show even larger structural fluctuations that get close to 0.8 nm and which may not be fully equilibrated after 400 ns (Figure 3B). Moreover, the conformational fluctuations of A10H and A13H involve the entire structure, which is again consistent with the large destabilization predicted by DUET (Table S1) and the more aggressive design of these mutations (introducing a bulky imidazole at a core location where there was only a methyl group). Therefore, we ruled out the A10H and A13H grafts for further study. For the other four grafts we extended the simulation time up to 750 ns (Figure S3) to ascertain whether the structural fluctuations (especially on L7H) would stabilize or continue evolving toward more unfolding. The longer trajectories showed small-scale reversible transitions with signs of stabilization around their characteristic mean values. From these combined results we decided to focus on L7H, M18H, F35H, and V40H as select grafts.

The Structural Environment of Select Grafts. Figure S4 shows the structural environment of the four gpW sites selected for histidine grafting. This figure highlights that L7 is

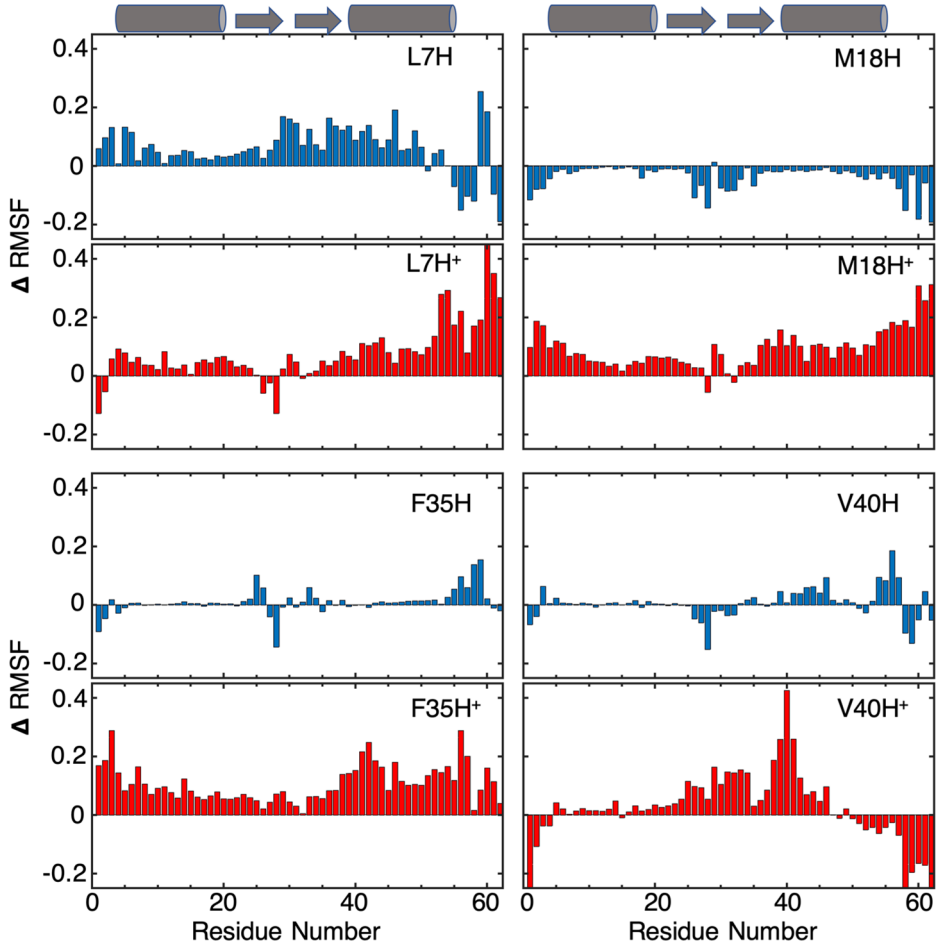

Figure 4. MD analysis of the structural fluctuations of gpW histidine grafts. The plots provide the difference in root-mean-square fluctuations (RMSF) per residue for each histidine graft. Blue represents the deprotonated simulations and red the protonated simulations relative to the wildtype trajectory.

https://dx.doi.org/10.1021/acssynbio.0c00190
ACS Synth. Biol. 2020, 9, 2427−2439

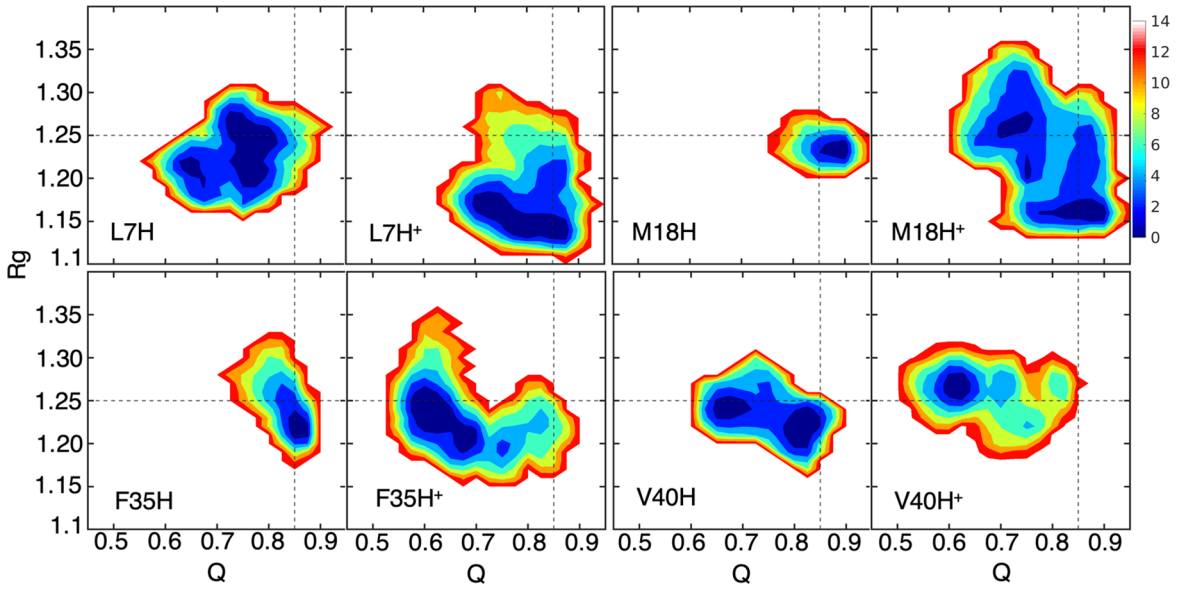

Figure 5. Conformational landscapes projected onto Q and R_g of the deprotonated and protonated trajectories at 310 K for each gpW histidine graft. The crossed dashed lines signal the wildtype gpW minimum for reference. The color bar provides the scale of $-RT \ln(p(Q, R_g))$ in kJ/mol.

buried and surrounded by nonpolar residues, but because leucine is bulky, mutation to histidine results on minor structural changes. M18 is solvent accessible, but it is surrounded by nonpolar residues, and the grafted histidine sits at the exposed/buried interface. F35 is embedded into the protein core formed between helix-2 and the β-hairpin. However, the designed histidine has plenty of room to fit the imidazole into the cavity left by the removed phenol. The mutation does affect the local electrostatic potential reflecting the slightly more polar nature of the imidazole ring. V40 is partially buried, and accordingly, its replacement by histidine results on a conservative mutation on a semiexposed core position with a slight increase in neighboring interactions of the bulkier side chain.

Enhanced Structural Fluctuations upon Histidine Ionization. We then examined the structural effects induced by histidine protonation *via* MD simulations in which the grafted histidine was kept protonated throughout the entire trajectory (see Methods). Particularly, we produced ∼2 μs of MD simulation for each of the protonated mutants. Relative to trajectories where the histidine is deprotonated, the protonated trajectories reveal generalized conformational rearrangements that take place in the submicrosecond time scale. As tool to examine the structural flexibility of the protonated and deprotonated trajectories, we calculated the time-averaged root-mean-square fluctuations (RMSF) of each protein residue along the trajectory. As reference, we performed the same analysis on the wildtype trajectory and calculate the RMSF difference relative to the wildtype (hence positive values imply that the residue is more flexible/unstructured than in the wildtype). The results of these calculations are shown in Figure 4. The deprotonated simulations indicate that M18H, F35H, and V40H are as conformationally stable in the subμs time scale as the wildtype. In contrast, MD simulations in protonated form show marked increases in structural fluctuations on the four grafts. For instance, M18H$^+$ loses tertiary interactions between the two α-helices, which triggers global unfolding. F35H$^+$ show similarly enhanced overall dynamics with increased flexibility of the residues in close contact with H35 (helix 2 residues 40−50). The F35H$^+$ trajectory shows the rupture of all tertiary interactions between the β-hairpin and helix-2 (the second gpW mini-core, Figure 1) *via* a sharp transition at ∼600 ns (Figure S5). The V40H$^+$ trajectory reveals a localized pattern of enhanced structural fluctuations around the mutated site that propagates into the hairpin, but the interactions between the protein termini appear stabilized. Finally, the L7H$^+$ ensemble shows enhanced fluctuations and partial unfolding, mostly of the end of helix-2 (residues 50−60), which forms tertiary interactions with helix-1 (where L7H is) that are weakened by histidine protonation. The most notable feature in L7H$^+$ is the opening of the hydrophobic core formed between the two helices in the native structure (see Figure S6). Overall these results provide computational evidence that there is effective thermodynamic coupling between histidine ionization and gpW unfolding in the four cases, which suggests that the grafts should be able to conformationally transduce changes in pH.

Conformational Landscapes of Neutral and Ionized Histidine Grafts. One characteristic of downhill folding is a gradual, minimally cooperative, unfolding behavior, which by face value seems consistent with the patterns that we see in MD simulations. To further investigate the nuanced effects of histidine grafting/ionization on gpW, we analyzed the trajectories in terms of projections onto two widely used order parameters: the fraction of native backbone contacts (Q) and the radius of gyration (R_g). Q informs on the overall degree of native structure that is made, and R_g informs on the degree of overall compaction of the polypeptide. The resulting conformational landscapes are shown in Figure 5. Even though conformational sampling might be somewhat limited, the projected landscapes are consistent with our previous conclusions from the RMSF analysis and provide further mechanistic insights. For instance, L7H significantly destabilizes the native ensemble, resulting in a decrease in Q relative to the wildtype's behavior (Figure S7). Interestingly, protonation (L7H$^+$) shifts the ensemble to slightly more native Q, but at the same time it makes it much more compact (lower R_g). This is so because breaking the helix−helix core exposes hydro-

https://dx.doi.org/10.1021/acssynbio.0c00190
ACS Synth. Biol. 2020, 9, 2427−2439

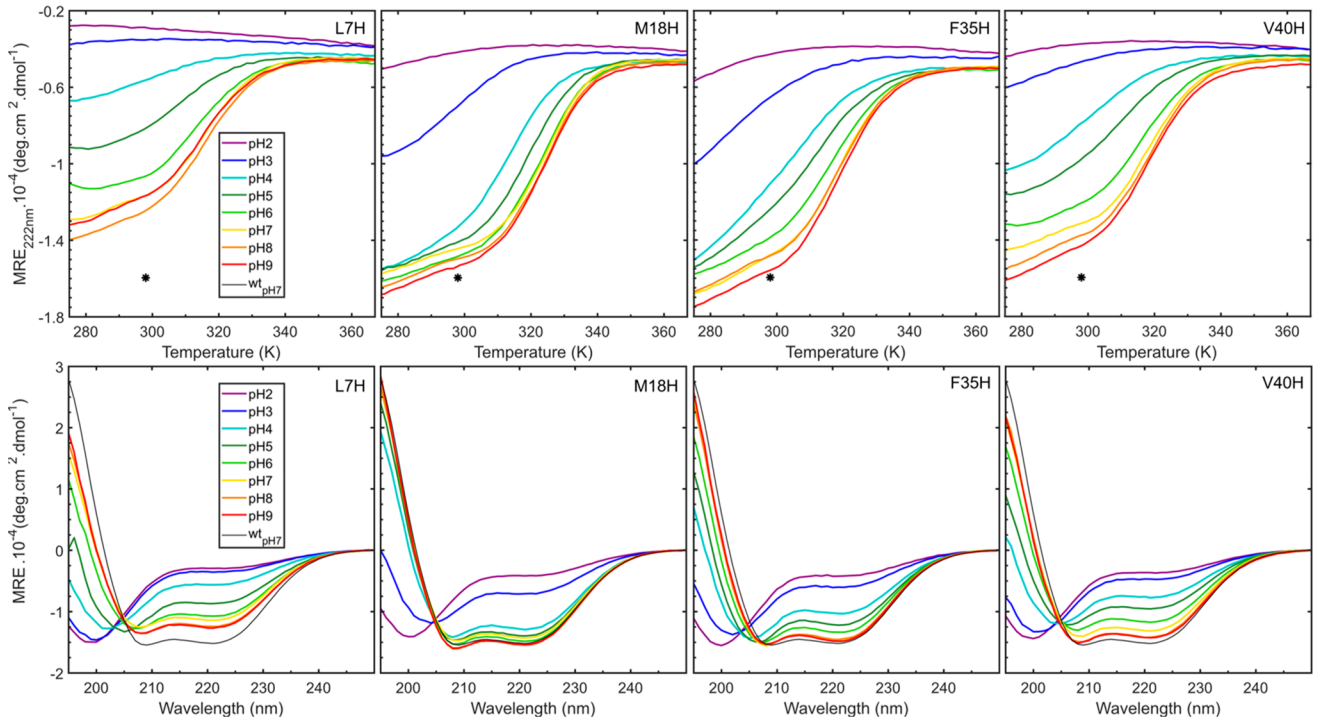

Figure 6. Temperature and pH unfolding of the four gpW histidine grafts. Each curve or spectrum is an average of 2 experiments. The curves and spectra are colored following the visible light spectrum, with the lowest pH corresponding to the highest energy (violet). The spectra at various pH values shown on the bottom row correspond to 298 K. The black asterisk on the top row indicates the unfolding curve of wildtype gpW at room temperature, pH 7. The spectrum shown as a thinner black line on bottom row panels corresponds to the wildtype at pH 7.

phobic surface, disorganizes the local helical conformation, and favors the collapse of the hairpin onto the newly exposed surface.

M18H behaves quite differently. In neutral form the ensemble is very similar to that of the wildtype. However, protonation produces a substantial loss in native contacts that points to extensive unfolding. The conformational ensemble of F35H is native-like in neutral form, but it experiences the most dramatic unfolding induced by protonation with $Q \sim 0.55$. We also noticed an increase in solvent-accessible surface area in the surrounding structural elements, which highlights the breakage of the two protein cores (Figure S6). The V40H graft has enhanced dynamics in neutral form, and extensive unfolding upon protonation, manifested by the loss of about 40% of the native contacts and a slightly more expanded ensemble (larger R_g). These observations further confirm the coupling between histidine ionization and native unfolding in these grafts. They also reveal that gpW unfolding starts locally and propagates from the graft to neighboring areas. Therefore, our computational results suggest that the engineered pH-induced unfolding of gpW is gradual, as expected for the downhill (un)folding scenario.

Experimental Analysis of Conformational pH Transducing. Figure 6 shows the unfolding of the four grafts as a function of pH and temperature measured by CD. From these data we can determine the destabilization induced by the mutation on gpW (*i.e.*, from data at pH 7), and the pH response of each graft. All mutations have a destabilizing effect on the native ensemble relative to the wildtype. The changes in free energy upon mutation are given in Table S2. As for the pH response, visual inspection reveals the loss of α-helical structure as pH becomes mildly acidic. For most of them the loss in structure is apparent even at pH 6. Overall, all grafts show enhanced disordering relative to the wildtype as pH drops from 8 to 4. On the other hand, the overall magnitude and response range of the pH effect varies widely between grafts, as we anticipated in our design strategy (see above). The pH response ranges from being minimally stronger than the wildtype's for M18H, to the rather dramatic response of L7H, which at pH 5 and room temperature already exhibits less native signal than the wildtype at pH 2. F35H and V40H have intermediate responses. Therefore, the experiments confirm the coupling between graft protonation and gpW unfolding.

A more detailed analysis requires taking into consideration that downhill (un)folding is gradual rather than an all-or-none process. The gradual character becomes most noticeable in double perturbation experiments, which result in the nonlinear coupling between the two perturbations (not obeying simple Maxwell relationships),[27] and also in changes in the pretransition baseline, or apparent native signal.[28,29] Double-perturbation effects have been previously reported for wildtype gpW in thermal-chemical perturbation experiments,[15] but are not readily apparent in its thermal-pH response because gpW is mostly insensitive to pH (Figure 2). However, nonlinear double perturbation effects are evident in the histidine grafts, both as a function of pH for each single graft (thermal-pH), or by comparing grafts with different stability (thermal-mutation). In general, the pretransition baseline for temperature denaturation drops as the pH lowers (*e.g.*, F35H in Figure 6 top), with the possible exception of M18H, which is the graft with the weakest pH transducing properties. It is of note that in native-like conditions (neutral pH and room temperature) L7H displays a 25% decrease in α-helical CD signal relative to the wildtype, consistently with the strongest pH response for this graft. pH also changes the degree of helical signal of the

https://dx.doi.org/10.1021/acssynbio.0c00190
ACS Synth. Biol. 2020, 9, 2427−2439

thermally unfolded state (*e.g.*, pH 2 unfolding curves in Figure 6 top), which becomes increasingly disordered (less negative CD at 222 nm) proportionally to the strength of the graft's pH response.

Importantly, the gradual unfolding of gpW coupled to histidine ionization results on transducers with varying response depending on the graft's location, and which exhibit broadband sensitivity relative to a conformational switch mechanism. This point was our working hypothesis, and the results from the four histidine grafts confirm it. There are two parameters to evaluate the performance of these conformational pH transducers: (1) the maximum signal difference, which defines the sensitivity of the transducer; (2) the dynamic range or response bandwidth, which defines the pH range that the transducer is sensitive to. Here we use the CD signal at 222 nm at room temperature as indicator of the transducer response. The data for the four grafts is given in Figure 7. This

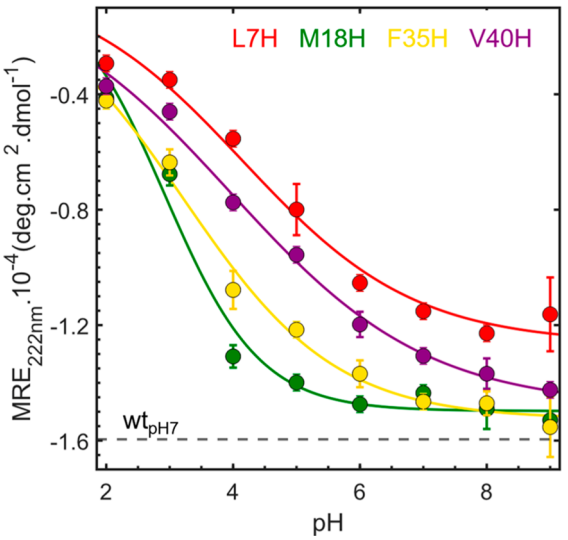

Figure 7. CD signal at 222 nm as a function of pH of all the single mutants at 298 K (circles) and their corresponding colored lines to guide the eye. The dashed line (--) represents the CD signal of wildtype gpW in its folded state (pH 7) as reference.

figure demonstrates that all single grafts are conformational pH transducers with sensitivity at pH > 4, whereas the wildtype is insensitive in that range (see Figure 2). Therefore, the histidine grafting approach works as general strategy to engineer conformational pH transducers into proteins. Figure 7 also highlights the broadband behavior of these transducers. As it was hinted in Figure 6 (bottom), the mutants feature significant differences in both the native (*i.e.*, high pH) and unfolded (at pH 2) CD signals. This behavior is due to the gradual (dis)ordering of downhill folding proteins in contrast to the interconversion between well-defined end-states of conformational switches. Interestingly, because the changes in the native and unfolded baselines go in the same direction (less negative ellipticity), the maximum signal change of the transducer is roughly invariant (about 11 000−12 000 deg cm^2 $dmol^{-1}$). In parallel, the dynamic range varies in a systematic way as a function of the graft. M18H has a dynamic range of about 3 pH units that is minimally extended over that of a switch transducer. Moreover, its sensitivity only spans the 2−5 pH range, which indicates that the perturbation from H18 ionization is not capable by itself of inducing the unfolding of gpW. M18H is also the mutant with highest stability in nonionized form (Table S1), which means it has a larger repository of folding free energy to compensate for the change in free energy upon histidine ionization. The next step up in dynamic range is F35H, which extends the response up to pH 6.5 and has maximal sensitivity around pH 4. V40H starts to show a slight decrease in native signal at neutral pH, and exhibits nearly linear CD signal changes over an impressively extended range of $[H^+]$ (from 10 nM to 10 mM, *i.e.*, pH 8−2). In other words, V40H is a distinct example of an ultra broadband pH transducer that could be used as foundation for implementing high performance pH sensors. L7H also has broadband pH response, but not as much because this mutant becomes fully unfolded at pH 3 and exhibits a fairly substantial loss in helical signal at neutral pH (see Figure 6 bottom), which penalizes its maximal signal difference (~9000 deg cm^2 $dmol^{-1}$). The pH response of these mutants, and particularly of L7H, highlights that the interplay between the intrinsic stability of the protein and the free energy perturbation upon ionization is key for the optimization of the dynamic range and maximum signal of rheostatic conformational transducers.

Reversibility of pH Transducing. An effective pH transducer should respond to pH changes in both directions and in fully reversible fashion. Routine control experiments in which we recorded the CD spectrum at room temperature of each graft before and after thermal denaturation (experiments on Figure 6 top) showed that the reversibility upon temperature denaturation was better than 95% for all grafts at all pH values tested (Figure S8). The reversibility after temperature denaturation is a very stringent test of the reversibility of protein unfolding transitions because high temperature enhances the aggregation of partially unfolded polypeptides.[30] As an additional control, we performed a simple test of reversibility of the pH transducing mechanism upon a drastic change in pH occurring at 293 K. The results from tests are shown in Figure 8 for the graft with the broadest

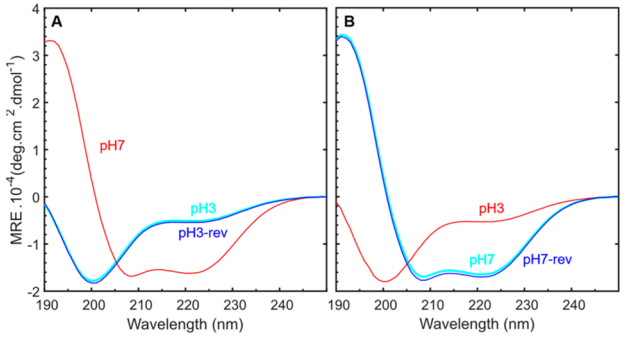

Figure 8. Reversible pH transducers. Far-UV CD spectrum of histidine graft V40H upon extreme changes in pH, both in neutralizing (A) and acidifying (B) directions at 293 K. The reversibility is shown on the V40H as example. Cyan signals the initial condition, red the changed condition, and dark blue the reversion to the initial condition.

dynamic range (V40H). The pH transducing mechanism exhibited excellent reversibility both when pH was changed from 3 to 7 and reverted back to 3, or when changed from 7 to 3 and reverted back to 7. These experiments demonstrate that the histidine grafts on gpW operate as reversible pH transducers.

https://dx.doi.org/10.1021/acssynbio.0c00190
ACS Synth. Biol. 2020, 9, 2427−2439

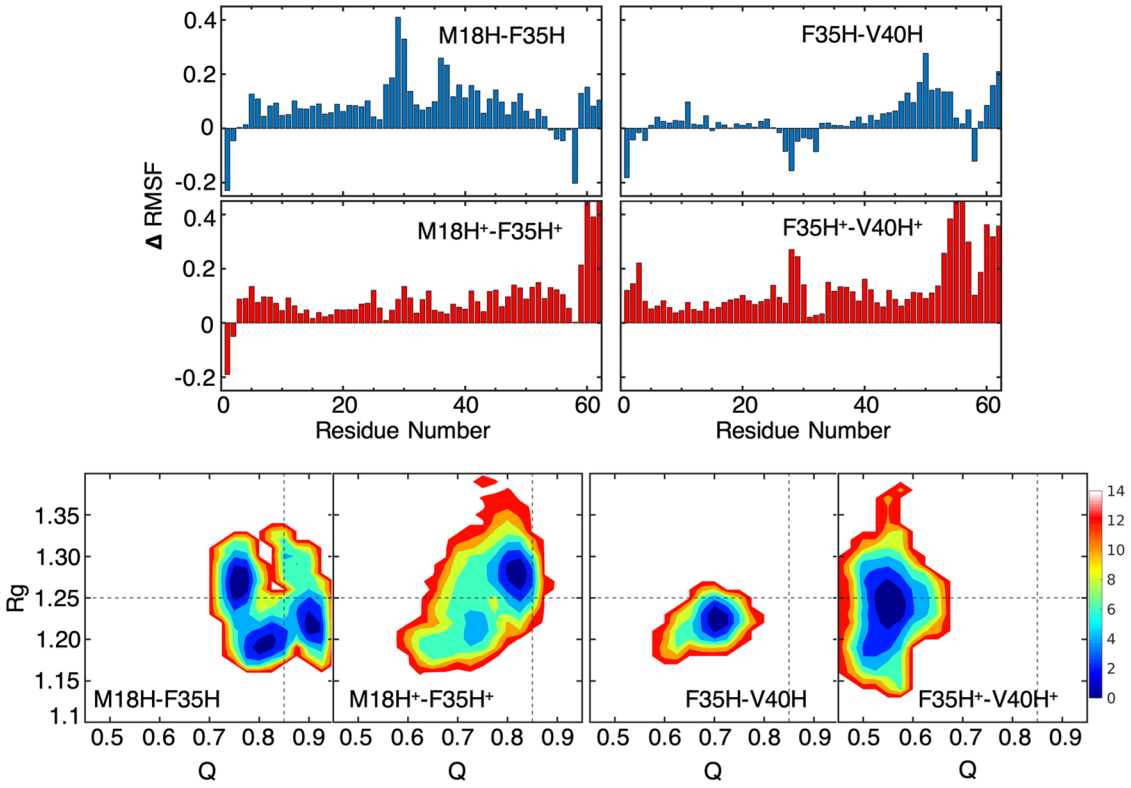

Figure 9. Computational analysis of double histidine grafts. (Top) ΔRMSF per residue for M18H−F35H and F35H−V40H in deprotonated (blue) and protonated (red) form. (Bottom) Conformational landscapes as a function of Q and R_g for each double mutant at 310 K. The color bar denotes the scale of $-RT \ln(p(Q, R_g))$ in kJ/mol. The crossing lines signal the minimum of the wildtype gpW simulation as reference.

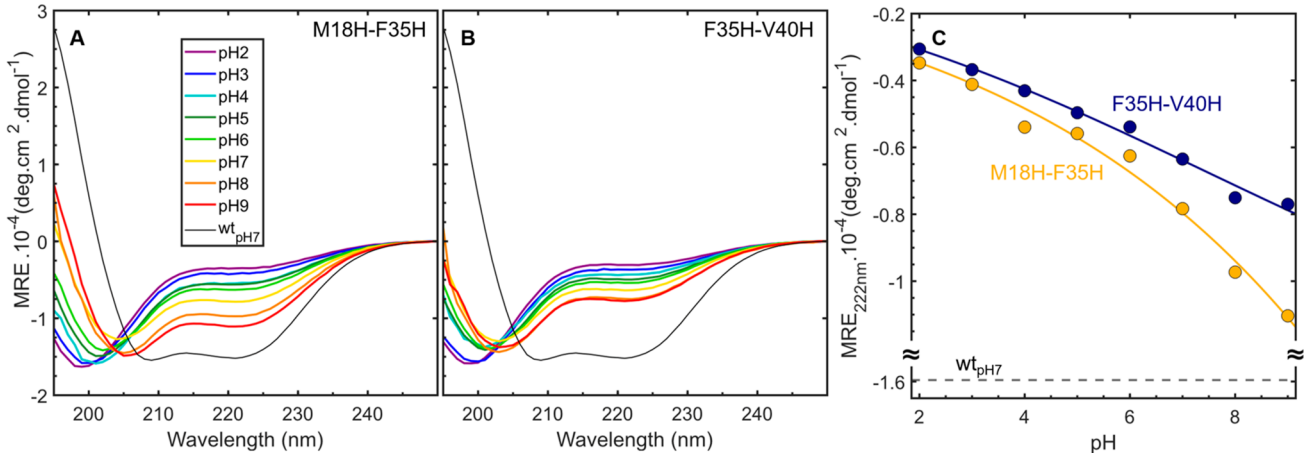

Figure 10. pH transducing on double histidine grafts. Far-UV CD spectra of the double histidine grafts M18H−F35H (A) and M18H−V40H (B) at 298 K as a function of pH. (C) CD signal at 222 nm as a function of pH for the double grafts (circles). The corresponding colored lines are to guide the eye. The dashed line (--) represents the CD signal at 222 nm of wildtype gpW at pH 7.

Modulating the Transducer Mechanism *via* Multiple Grafts. Our results indicate that the response of the pH transducer depends on the structural environment of the histidine graft: more buried positions lead to broader dynamic range. The question remaining is whether the effects of more than one graft are additive or exhibit positive or negative cooperativity. We decided to explore this issue by producing double grafts. However, we had to be careful as the single gpW grafts are already marginally stable (Table S2). We ruled out L7H since it is already at the brink of native stability, and targeted M18H−F35H as a conservative double graft and F35H−V40H as a more aggressive one (based on Figure 7 and Table S2).

As we did for the single grafts, we first analyzed the conformational behavior of the double grafts *in silico*. The increased perturbation without ionization of the double mutants is evident in the RMSF analysis (Figure 9 top). Ionization of the double grafts produces enhanced RMSF, particularly for F35H−V40H, in line with what we expected from our experimental data on the pH response of the single mutants (Figures 6, 7). The conformational landscapes of the double grafts confirm that both are marginally stable in their deprotonated forms and undergo large unfolding upon double

https://dx.doi.org/10.1021/acssynbio.0c00190
ACS Synth. Biol. 2020, 9, 2427−2439

histidine ionization (Figure 9 bottom). The degree of disordering is particularly evident for F35H$^+$−V40H$^+$, amounting to ∼50% loss in native contacts.

The experimental analysis of the double grafts highlights a slightly different pH response, which provides further insight into the coupling between downhill (un)folding and proton binding. Particularly, the maximum α-helical signal (at the highest pH) is reduced, and it only reaches 70% of the wildtype native signal for M18H−F35H (Figure 10A) and 50% for F35H−V40H (Figure 10B). As a result, the CD signal at 222 nm has a convex dependence with pH (Figure 10C), rather than the sigmoidal-concave dependence of the single grafts. The reason behind these differences is that the double mutants are already partially unfolded at room temperature, even when the histidine residues are deionized. Therefore, histidine ionization can only tilt the already partially unfolded ensemble toward more disorder, hence resulting on the convex pH dependence shown in Figure 10C (half of a broad negative sigmoidal curve). The partially disordered native-like ensembles of the double grafts are most evident when compared with the CD spectrum of the wildtype gpW at neutral pH (Figures 10A,B). This result is consistent with the quantitative analysis of their thermal denaturation at neutral pH, which indicates that at room temperature both of these proteins are close to, or just past the denaturation midpoint (Table S2). In terms of their properties as conformational pH transducers, the double mutants feature a reduction in maximum CD signal that is concomitant to their marginal intrinsic stability (7500 and 5000 deg cm^2 dmol^{-1}, respectively). On the other hand, their response is fairly linear over the full pH range (2−9), which indicates that the double grafts in conjunction with a marginally stable nonionized downhill folding scaffold result in lower sensitivity, but also on ultrabroadband pH transducers.

Lessons for Engineering Protein-Based Conformational Transducers. We have explored a strategy for engineering conformational transducers for biosensor applications based on thermodynamically coupling the (un)folding process of a downhill folding protein domain to the binding of an analyte of interest. The underlying hypothesis was that such coupling might give rise to rheostatic (analog) rather than switching (binary) conformational transducers.[10] As protein scaffold we chose the fast, downhill folder gpW, pH as analyte, and histidine grafting as an approach to engineer the conformational transducer.

A first observation is that the histidine grafting strategy we used introduces sensitivity to pH in the mildly acidic to neutral range in a systematic way. pH sensitivity results from the thermodynamic coupling between imidazole ionization and protein unfolding. We find that the strategy is customizable by selecting the degree of histidine burial and the number of grafts. The key for a successful pH transducer is to balance out the repository of folding free energy existing in the scaffold with the perturbation induced by histidine(s) ionization (pK_a shifts) so that the protein undergoes reversible unfolding at the desired pH range. This delicate trade-off is a key parameter to define the transducer's performance. When the folding free energy repository is larger the transducer's response becomes sharper (*e.g.*, M18H, Figure 7). On the other hand, when the repository is very small the response is broadest, but the amplitude of the signal inevitably drops (*e.g.*, F35H−V40H, Figure 10). For the gpW scaffold the optimal pH transducing response appears to be for grafts with a folding free energy repository of about 5 kJ/mol (*e.g.*, V40H, Figure 7). The right balance can be attained by combining the (de)stabilization of the scaffold's native structure *via* site-directed mutagenesis and the structure-based design of the histidine grafts.

These lessons from the histidine grafting approach should be extrapolatable to the engineering of conformational transducers for analytes that require a structurally defined binding site. In such cases, the most straightforward approach could be to engineer the folding properties of a protein domain that already contains the binding site for the target ligand. Using protein engineering, one could then tune its sequence to make it both inherently unstable and downhill-like (*i.e.*, by enhancing secondary structure propensity and weakening the hydrophobic core[5,10]), and balancing the overall perturbation so that it folds gradually upon binding to the ligand (folding upon binding transducer). In that regard, the combination of computational and experimental methods that we use here can prove quite useful. The structural−stereochemical rules that we have used for the design of histidine grafts are straightforward and extensible. MD simulations in the few microseconds time scale seem to recapitulate the conformational effects induced by local perturbations (mutation and ionization), at least for microsecond folding domains such as gpW. We also find good agreement between the results from the simulations and the experimental characterization of the histidine grafts, which opens the possibility of using computational methods to screen larger collections of mutants before producing and characterizing them in the lab. A general approach to engineer rheostatic conformational transducers for other analytes could then involve the following: (1) identification of a protein scaffold that naturally binds to the analyte; (2) structure-based design of mutations to decrease folding cooperativity and reduce native stability; (3) mutational screening *via* molecular simulations; and (4) production and experimental characterization of most promising candidates.

Downhill (Un)Folding Coupled to Binding: Implications for Broadband Transducing. Our results shed light into the interplay between downhill (un)folding and binding and how it can give rise to conformational transducers with special properties. We can extract several practical lessons. First, the coupling between histidine ionization and downhill (un)folding converts the destabilization directly into structural changes. This feature is inherent to downhill (un)folding domains, which have flexible native ensembles, and gradual (continuous) unfolding transitions. Therefore, even relatively minor free energy perturbations result in structural changes that can be detected. In other words, the structural changes are not limited to the interconversion between a native and an unfolded state, but also involve the gradual (dis)ordering of these ensembles.

An important implication of such gradual behavior is the implementation of rheostatic conformational transducers that are responsive over unprecedentedly broad ranges of ligand concentration. To illustrate this point, it is useful to compare the response shown in Figures 7 and 10 with a conformational switch mechanism. Conformational switches transduce signals by toggling between their end states (*e.g.*, native and unfolded) in response to the binding/release of the ligand. Their response is directly proportional to the fraction bound, which practically limits their response to within a factor of 20 below and above the apparent K_d or C_{50}, that is, to site occupancies between 0.05 and 0.95. Outside of that range the

https://dx.doi.org/10.1021/acssynbio.0c00190
ACS Synth. Biol. 2020, 9, 2427−2439

changes in ligand chemical potential do not translate into significant changes in population, so the transducer's response flattens. In contrast, the pH transducers we have engineered into gpW, whether single or double grafts, exhibit conformational changes that extend well beyond the 2.5 orders of magnitude. Interestingly, the dynamic range in pH sensitivity increases proportionally to the magnitude of the perturbation produced by ionization (Figure 7). The dynamic range eventually extends over 7 orders of magnitude in $[H^+]$, resulting in ultrabroadband pH transducers. Such transducers would offer impressive improvements over the dynamic range of existing pH sensors.[31]

However, the outstanding potential for broadband sensing comes with a price in signal sensitivity. The conformational transitions of downhill folders are still constrained within well-defined structural extremes: a native 3D structure and a random-coil ensemble. Moreover, due to their marginal cooperativity, under mild conditions downhill folders rarely reach either end state,[27] which reduces the maximum signal change that can be induced. Practically, the relevant measure of sensitivity is the ratio between signal change and ligand concentration, which is inversely proportional to the dynamic range. In other words, the broader the dynamic range, the lower the sensitivity. Moreover, whereas CD is a convenient method to probe the conformation of proteins (particularly of α-helical ones), its inherently low sensitivity and specificity add to the challenges of implementing conformational rheostatic biosensors with sufficient sensitivity. One possibility to surmount these limitations might be to introduce a signal gain mechanism by coupling the conformational change of the downhill scaffold to an amplifiable, high sensitivity readout, such as fluorescence and/or electrical signals. To really exploit the gradual response of conformational rheostats the reporter signal should ideally change proportionally to the structural change rather than in binary fashion. One option are fluorescence readouts based on Förster resonance energy transfer between donor and acceptor fluorophores, which changes in efficiency proportionally to the interdye distance in the $R_0 - 1$ nm to $R_0 + 1$ nm range (where R_0 is the characteristic distance at which the efficiency is 0.5).[32]

Technical challenges notwithstanding, we can conclude that rheostatic conformational transducers add a new, exciting tool to the biosensor engineering toolbox. The sharp response of switching transducers will be preferable for applications where the range in ligand concentration is narrow and minor changes in ligand levels must be detected. An example of ultrasharp response are physiological temperature sensors, which need to detect changes of even a fraction of a degree. On the other hand, rheostatic transducers could provide improved performance to monitor signals that vary widely. For instance, pH changes between 8 and 4 inside living cells statically and dynamically, depending on the cellular compartment[33] and/or the cell's metabolic status. Currently, there are intracellular pH sensors (fluorophore-based and fluorescent protein-based) for either the neutral or the acidic (lysosomal) ranges.[34] However, there are no pH sensors available that can simultaneously operate in all intracellular locations and/or all metabolic stages, even though this capability is widely recognized as essential to understand the role of pH homeostasis in cell biology and physiology.[35] Another example of broadband biological signal is the second messenger Ca^{2+}, which is found at only 50 nM in the cytosol, 500 μM in the ER, and at mM levels extracellularly, and which changes drastically and very quickly (sub-ms) in response to variate inputs.[36] Here again there are chemical and recombinant (*e.g.*, calmodulin-based) Ca^{2+} sensors available,[37−39] but none of them get close to covering the vast physiological $[Ca^{2+}]$ range nor the fast, local concentration spikes arising from signaling pulses, such as those associated with cell contractility.[40] Conformational rheostat transducers would be, in this respect, tremendously useful as a means to enable the broadband sensing required to effectively track widely varying biological signals/properties, such as Ca^{2+} and pH.

METHODS

Computational Methods. *Design Strategy.* To design mutations to histidine in core positions with varying degree of solvent exposure of the protein gpW (PDB ID: 2L6Q), we used the Chimera tool and DUET algorithm.[41] A combination of structural analysis to identify target locations and stereochemical criteria were used to identify conservative replacements to histidine (*e.g.*, with enough room to accommodate the imidazole ring). Target mutation sites were ranked according to the predicted change in stability upon mutation calculated with DUET. The six single point mutations to histidine were designed with the Chimera tool and refined *via* energy minimization. The fully solvent accessible histidine 15 in gpW was also replaced to Ala to investigate the effects of ionization of the natural histidine. As further computational test of the intrinsic native stability, all-atom MD trajectories in explicit solvent were run for each mutant in deprotonated form as well as for wildtype gpW (see below).

Electrostatic Potential Calculations. The electrostatic potential maps of gpW and its mutants were calculated at physiological conditions (pH 7) using the adaptive Poisson−Boltzmann solver (APBS).[42] The input PQR files were generated by the PDB2PQR server using the PARSE forcefield and the protonation states were assigned by PROPKA. The grid dimensions were automatically set by APBS based on the input structure. Electrostatic potentials were calculated by solving the linear Poisson−Boltzmann equation with a single DH sphere boundary condition. The solvent accessible surface area was calculated using a solvent radius of 1.4 Å.

All Atom MD Simulations. MD simulations were performed in the GROMACS suite[43] using the OPLS all-atom force field.[44] Water molecules were modeled with the TIP4P representation.[45] Periodic boundary conditions were used, and long-range electrostatic interactions were treated with the Particle Mesh Ewald (PME) summation using a grid spacing of 0.16 nm combined with a fourth-order cubic interpolation to derive the potential and forces in-between grid points.[46] The real space cutoff distance was set to 1.0 nm and the van der Waals cutoff to 1.0 nm. The bond lengths were fixed[47] and a time step of 2 fs was used for numerical integration of the equations of motion. Coordinates were recorded every 10 ps. The simulations were performed at 310 K starting from the coordinates of the lowest energy conformer in the gpW NMR structural ensemble modified to carry the mutations to histidine and the H15A pseudo-wildtype. The protein was placed in a dodecahedral water box large enough to contain protein and at least 1.0 nm of solvent on all sides (volume ~233 nm^3). The structure was solvated with ~7300 water molecules, and 4−5 Cl^- ions were added to neutralize the system. The starting structure was subjected to energy minimization using the steepest descent method. All systems were equilibrated at a constant temperature of 310 K utilizing

https://dx.doi.org/10.1021/acssynbio.0c00190
ACS Synth. Biol. 2020, 9, 2427−2439

the two-step ensemble process (NVT and NPT). First, the system was subjected to NVT (constant number of particles, volume, and temperature) equilibration for 100 ps with the position of the protein restrained, followed by NPT (constant number of particles, pressure and temperature) equilibration for another 100 ps. The simulations were subjected to the modified Berendsen thermostat with 0.1 ps relaxation time to maintain the exact temperature,[48] followed by Parrinello−Rahman[49] with 0.2 ps relaxation time for pressure coupling at 1 bar before the production run was started. All the simulations were run on the Triton Shared Computing Cluster (TSCC) at the San Diego Supercomputing center (SDSC). The total simulation time per variant was 1 μs for the wildtype, 0.75 μs for the mutants L7H, M18H, F35H, and V40H, and 0.4 μs for A10H and A13H.

MD Simulations of Mildly Acidic Conditions. All the protonated mutant MD trajectories ($L7H^+$, $M18H^+$, $F35H^+$, and $V40H^+$) were run for 2.2 μs. In absence of well-established methodology to define and control pH during MD simulations (simulations do not contain free hydronium ions and protons cannot be exchanged in classical MD) we altered the protonation state of all titratable residues before the MD run based on their estimated pK_a values and relative to a nominal pH of 5. The ionization states were kept constant for the entire MD run. Histidine protonation was carried out using the pdb2gmx tool (HISE type) by first performing a standard pK_a calculation of the starting structure using Delphipka.

MD Simulations of Double His-Grafts. MD simulations were carried out in deprotonated and protonated form for two double histidine grafts: M18H−F35H and F35H−V40H. Each double mutant was simulated for 1 and 2.2 μs in the deprotonated and protonated forms, respectively.

Analysis of MD Trajectories. The root-mean-square fluctuations (RMSF) per residue were calculated for each MD trajectory (protonated, deprotonated, and wildtype) using the gmx rmsf tool. The RMSF of each mutant trajectory was expressed in reference to the wildtype as ΔRMSF ($RMSF_{mut} - RMSF_{wt}$).

Conformational Landscapes of gpW Mutants. Maps were obtained from the normalized probability distribution as a function of the relevant set of order parameters. The probability distribution was converted into an energy scale using the following expression:

$$\Delta A_{\mathrm{ref}\rightarrow i} = -RT \ln(p_i/p_{\mathrm{ref}})$$

where the probability of going from a reference state (ref) of the system to any state i (*e.g.*, from folded to unfolded) at constant temperature and constant volume is evaluated. R is the ideal gas constant, T is the temperature and p_i and p_{ref} are the probabilities of finding the system in state i and state *ref*, respectively. We project the conformational space onto two order parameters: the radius of gyration (R_g) and the fraction of native backbone contacts (Q). In this calculation a contact is considered formed when the minimum pairwise distance between atoms of the interacting residues is ≤0.55 nm and the residue pair is >3 residues apart in the protein sequence. Conformations collected at 100 ps intervals were projected onto the Q−R_g plane using a 20 × 20 grid (400 cells) and sampling statistics were compiled to evaluate $\Delta A_{\mathrm{ref}\rightarrow i}$. The grid cell with the largest population was used as reference state.

Experimental Methods. *Recombinant Protein Expression.* All gpW variants including the wild type, single mutants and double mutants were produced by recombinant means. Wildtype gpW and the single His mutants were cloned as full genes in the bacterial expression vector pBAT4. Double His mutants were cloned as SUMO-His-tag fusions to improve protein expression and facilitate expression of these unstable mutants. Plasmids containing the various gpW genes were transformed into *E. coli* BL21(DE3) competent cells. Cells were grown in LB broth at 310 K until the optical density at 600 nm reached a value of 1.0−1.2 followed by induction with isopropyl-β-D-thio-galactopyranoside (IPTG). After IPTG addition, cells were kept in growing conditions at 310 K for 4 h and then harvested and centrifuged at 8000 rpm for 30 min. The pellets were resuspended until homogeneous in the buffer required for protein purification. Cell lysis was performed using the freeze−thaw method (6 cycles). The lysates were subjected to ultracentrifugation at 35 000 rpm for 30 min.

Protein Purification. The supernatant obtained after ultracentrifugation was loaded onto a HPLC HiTrap SP cation exchange column (GE Healthcare) and eluted with a gradient from 0 to 1 M NaCl in 20 mM phosphate buffer at pH 6.5. The fractions containing the gpW protein variant were pooled and subjected to a second round of HPLC purification on a reverse phase (RP) column using a 0−95% Acetonitrile gradient with 0.1% trifluoroacetic acid (TFA) for elution. Double His mutants (SUMO-His-tag fusions) were purified with a first step of affinity chromatography by loading the sample onto a Nickel Column (His-Trap) followed by washing with binding buffer (20 mM Tris pH 7.5, 150 mM NaCl, and 10 mM Imidazole), and elution with a gradient from 0% to 100% elution buffer (20 mM Tris pH 7.5, 150 mM NaCl, and 500 mM Imidazole). The protein tags were cleaved using ULP1 by incubation at 277 K overnight, and subsequently removed by a second pass through the Nickel column, (His-Trap) followed by Reverse Phase chromatography (as above). All fractions containing pure gpW variant were pooled, lyophilized, and stored at 253 K. Protein purity was assessed by sodium dodecyl sulfate polyacrylamide gel electrophoresis, and mutant identity verified by electrospray mass spectrometry.

Far-UV Circular Dichroism (CD) Spectroscopy. All the protein samples were prepared at 30 μM concentration in 20 mM buffer by dilution from 300 μM stocks prepared in the same buffer. Citrate buffer was used for experiments in the 3−6 pH range. Phosphate buffer was used for pH 7, and Tris-HCl buffer for the 8−9 pH range. HCl in water was used to prepare samples at pH 2. CD spectra were measured from 195 to 250 nm with 1 nm resolution and 2 nm effective bandwidth. Thermal denaturation curves monitored by CD were performed on a Chirascan CD spectrometer from Applied Photo Physics equipped with a temperature controller system. A cuvette with a path length of 1 mm was used. Thermal denaturation experiments were performed recording CD spectra every 2 K from 273 to 373 K. CD spectra were baseline subtracted (spectrum of the same buffer). All experiments were done in duplicate. The relative final protein concentration of all samples for each gpW variant were calculated using a two-step procedure to minimize errors due to the small molar extinction coefficient of gpW at 280 nm: (1) concentrations were estimated from the stock solution concentration determined by absorbance at 280 nm (gpW has one tyrosine, ε(280 nm) = 1280 M^{-1} cm^{-1}) after applying the corresponding dilution factor; and (2) a correction factor based on the ratio of the absorbance at 195 nm (ε(195 nm) ≈

https://dx.doi.org/10.1021/acssynbio.0c00190
ACS Synth. Biol. 2020, 9, 2427−2439

300 000 M^{-1} cm^{-1}) of the sample relative to that of an internal reference (wildtype gpW at pH 2) was applied to minimize pipetting errors.

Reversibility Test of pH-Induced Protein (Un)Folding. The far UV-CD spectrum of the samples was recorded from 190 to 250 nm at 293 K. The initial samples were prepared by dissolving lyophilized protein in water at a concentration of 30 μM in a microcentrifuge tube. The pH was adjusted by adding either NaOH (0.01 M or 0.1M) or HCl (0.01 M or 0.1M) in 1 μL steps until reaching the desired pH value (3 or 7). The sample was transferred to the CD cuvette, temperature equilibrated for 10 min and the spectrum was acquired. The solution was then transferred back to the microcentrifuge tubes and adjusted to the other extreme pH (7 or 3) adding NaOH or HCl in 1 μL steps measuring the final pH with an ultrathin electrode. The sample was retransferred to the CD cuvette for spectrum measurement. After acquisition the entire process was repeated adjusting the pH back to the original value (3 or 7) adding HCl or NaOH in 1 μL steps and recording the CD spectrum at the reversed pH. The added volumes were recorded and used to correct for the actual changes in protein concentration. The entire procedure was done three times, and the triplicated spectra averaged.

■ ASSOCIATED CONTENT

Supporting Information

The Supporting Information is available free of charge at https://pubs.acs.org/doi/10.1021/acssynbio.0c00190.

Supplementary tables with the changes in stability as predicted by DUET (S1) or measured experimentally (S2), and figures with the wildtype gpW changes in midpoint temperature as a function of pH (Figure S1), the per residue solvent accessible surface area (Figure S2), the RMSD time evolution of the MD trajectories (Figure S3), the structural environment of the four histidine grafts (Figure S4), the evolution of residue−residue interacting pairs between β-hairpin and α-helix-2 along the F35H$^+$ trajectory (Figure S5), the distribution of solvent accessible surface area for the four histidine grafts (Figure S6), the conformational landscape of wild type gpW from MD simulations (Figure S7), and the CD spectra of all proteins (wt, 4 single grafts and 2 double grafts) before and after the thermal denaturation experiments at pH 7 and 3 (Figure S8) (PDF)

■ AUTHOR INFORMATION

Corresponding Author

Victor Muñoz − *Bioengineering Graduate Program, NSF-CREST Center for Cellular and Biomolecular Machines (CCBM), Chemistry and Chemical Biology Graduate Program, and Department of Bioengineering, University of California at Merced, Merced 95343, California, United States;* orcid.org/0000-0002-5683-1482; Email: vmunoz3@ucmerced.edu

Authors

Suhani Nagpal − *Bioengineering Graduate Program and NSF-CREST Center for Cellular and Biomolecular Machines (CCBM), University of California at Merced, Merced 95343, California, United States*

Thinh D. N. Luong − *NSF-CREST Center for Cellular and Biomolecular Machines (CCBM) and Chemistry and Chemical Biology Graduate Program, University of California at Merced, Merced 95343, California, United States;* orcid.org/0000-0001-7128-6921

Mourad Sadqi − *NSF-CREST Center for Cellular and Biomolecular Machines (CCBM) and Department of Bioengineering, University of California at Merced, Merced 95343, California, United States*

Complete contact information is available at: https://pubs.acs.org/10.1021/acssynbio.0c00190

Author Contributions

#S.N. and T.L. have contributed equally to this work.

Notes

The authors declare no competing financial interest.

■ ACKNOWLEDGMENTS

This work was supported by the W. M. Keck Foundation. V.M. acknowledges additional support from the European Research Council (grant ERC-2012-ADG- 323059), the National Science foundation (NSF-MCB-1616759), and the CREST Center for Cellular and Biomolecular Machines (grant NSF-CREST-1547848).

■ REFERENCES

(1) Vallee-Belisle, A., and Plaxco, K. W. (2010) Structure-switching biosensors: inspired by Nature. *Curr. Opin. Struct. Biol. 20*, 518−526.

(2) Plaxco, K. W., and Soh, H. T. (2011) Switch-based biosensors: a new approach towards real-time, in vivo molecular detection. *Trends Biotechnol. 29*, 1−5.

(3) Ha, J.-H., and Loh, S. N. (2012) Protein conformational switches: from nature to design. *Chem. - Eur. J. 18*, 7984−7999.

(4) Vallée-Bélisle, A., Ricci, F., and Plaxco, K. W. (2009) Thermodynamic basis for the optimization of binding-induced biomolecular switches and structure-switching biosensors. *Proc. Natl. Acad. Sci. U. S. A. 106*, 13802.

(5) De Sancho, D., and Muñoz, V. (2011) Integrated prediction of protein folding and unfolding rates from only size and structural class. *Phys. Chem. Chem. Phys. 13*, 17030−17043.

(6) Muñoz, V. (2007) Conformational dynamics and ensembles in protein folding. *Annu. Rev. Biophys. Biomol. Struct. 36*, 395−412.

(7) Garcia-Mira, M. M., Sadqi, M., Fischer, N., Sanchez-Ruiz, J. M., and Muñoz, V. (2002) Experimental Identification of Downhill Protein Folding. *Science 298*, 2191.

(8) Sadqi, M., Fushman, D., and Muñoz, V. (2006) Atom-by-atom analysis of global downhill protein folding. *Nature 442*, 317−321.

(9) Naganathan, A. N., and Muñoz, V. (2014) Thermodynamics of Downhill Folding: Multi-Probe Analysis of PDD, a Protein that Folds Over a Marginal Free Energy Barrier. *J. Phys. Chem. B 118*, 8982−8994.

(10) Muñoz, V., Campos, L. A., and Sadqi, M. (2016) Limited cooperativity in protein folding. *Curr. Opin. Struct. Biol. 36*, 58−66.

(11) Li, P., Oliva, F. Y., Naganathan, A. N., and Muñoz, V. (2009) Dynamics of one-state downhill protein folding. *Proc. Natl. Acad. Sci. U. S. A. 106*, 103−108.

(12) Cerminara, M., Desai, T. M., Sadqi, M., and Muñoz, V. (2012) Downhill protein folding modules as scaffolds for broad-range ultrafast biosensors. *J. Am. Chem. Soc. 134*, 8010−8013.

(13) Sborgi, L., Verma, A., Muñoz, V., and de Alba, E. (2011) Revisiting the NMR structure of the ultrafast downhill folding protein gpW from bacteriophage lambda. *PLoS One 6*, e26409.

(14) Sborgi, L., Verma, A., Piana, S., Lindorff-Larsen, K., Cerminara, M., Santiveri, C. M., Shaw, D. E., de Alba, E., and Muñoz, V. (2015) Interaction Networks in Protein Folding *via* Atomic-Resolution Experiments and Long-Time-Scale Molecular Dynamics Simulations. *J. Am. Chem. Soc. 137*, 6506−6516.

(15) Fung, A., Li, P., Godoy-Ruiz, R., Sanchez-Ruiz, J. M., and Muñoz, V. (2008) Expanding the realm of ultrafast protein folding:

gpW, a midsize natural single-domain with alpha+beta topology that folds downhill. *J. Am. Chem. Soc. 130*, 7489−7495.
(16) White, K. A., Ruiz, D. G., Szpiech, Z. A., Strauli, N. B., Hernandez, R. D., Jacobson, M. P., and Barber, D. L. (2017) Cancer-associated arginine-to-histidine mutations confer a gain in pH sensing to mutant proteins. *Sci. Signaling 10*, eaam9931.
(17) Deochand, D. K., Perera, I. C., Crochet, R. B., Gilbert, N. C., Newcomer, M. E., and Grove, A. (2016) Histidine switch controlling pH-dependent protein folding and DNA binding in a transcription factor at the core of synthetic network devices. *Mol. BioSyst. 12*, 2417−2426.
(18) Perier, A., Chassaing, A., Raffestin, S., Pichard, S., Masella, M., Ménez, A., Forge, V., Chenal, A., and Gillet, D. (2007) Concerted Protonation of Key Histidines Triggers Membrane Interaction of the Diphtheria Toxin T Domain. *J. Biol. Chem. 282*, 24239−24245.
(19) Narayan, A., and Naganathan, A. N. (2018) Switching Protein Conformational Substates by Protonation and Mutation. *J. Phys. Chem. B 122*, 11039−11047.
(20) Malevanets, A., Chong, P. A., Hansen, D. F., Rizk, P., Sun, Y., Lin, H., Muhandiram, R., Chakrabartty, A., Kay, L. E., Forman-Kay, J. D., and Wodak, S. J. (2017) Interplay of buried histidine protonation and protein stability in prion misfolding. *Sci. Rep. 7*, 882.
(21) Boyken, S. E., Benhaim, M. A., Busch, F., Jia, M., Bick, M. J., Choi, H., Klima, J. C., Chen, Z., Walkey, C., Mileant, A., Sahasrabuddhe, A., Wei, K. Y., Hodge, E. A., Byron, S., Quijano-Rubio, A., Sankaran, B., King, N. P., Lippincott-Schwartz, J., Wysocki, V. H., Lee, K. K., and Baker, D. (2019) De novo design of tunable, pH-driven conformational changes. *Science 364*, 658.
(22) Yildiz, Ö., Vinothkumar, K. R., Goswami, P., and Kühlbrandt, W. (2006) Structure of the monomeric outer-membrane porin OmpG in the open and closed conformation. *EMBO J. 25*, 3702−3713.
(23) Edgcomb, S. P., and Murphy, K. P. (2002) Variability in the pKa of histidine side-chains correlates with burial within proteins. *Proteins: Struct., Funct., Genet. 49*, 1−6.
(24) Crooks, J. E., Hibbert, F., and Willi, A. V. (1977) *Proton Transfer*, Elsevier, Amsterdam.
(25) Muñoz, V., and Cerminara, M. (2016) When fast is better: protein folding fundamentals and mechanisms from ultrafast approaches. *Biochem. J. 473*, 2545−2559.
(26) Chaudhury, S., Ripoll, D. R., and Wallqvist, A. (2015) Structure-based pKa prediction provides a thermodynamic basis for the role of histidines in pH-induced conformational transitions in dengue virus. *Biochem. Biophys. Rep. 4*, 375−385.
(27) Oliva, F. Y., and Muñoz, V. (2004) A Simple Thermodynamic Test To Discriminate between Two-State and Downhill Folding. *J. Am. Chem. Soc. 126*, 8596−8597.
(28) Naganathan, A. N., Perez-Jimenez, R., Sanchez-Ruiz, J. M., and Muñoz, V. (2005) Robustness of downhill folding: guidelines for the analysis of equilibrium folding experiments on small proteins. *Biochemistry 44*, 7435−7449.
(29) Naganathan, A. N., and Muñoz, V. (2008) Determining denaturation midpoints in multiprobe equilibrium protein folding experiments. *Biochemistry 47*, 6752−6761.
(30) Ibarra-Molero, B., Naganathan, A. N., Sanchez-Ruiz, J. M., and Muñoz, V. (2016) Modern analysis of protein folding by differential scanning calorimetry. *Methods Enzymol. 567*, 281−318.
(31) Richardson, D. S., Gregor, C., Winter, F. R., Urban, N. T., Sahl, S. J., Willig, K. I., and Hell, S. W. (2017) SRpHi ratiometric pH biosensors for super-resolution microscopy. *Nat. Commun. 8*, 577.
(32) Stryer, L. (1978) Fluorescence energy transfer as a spectroscopic ruler. *Annu. Rev. Biochem. 47*, 819−846.
(33) Casey, J. R., Grinstein, S., and Orlowski, J. (2010) Sensors and regulators of intracellular pH. *Nat. Rev. Mol. Cell Biol. 11*, 50−61.
(34) Han, J., and Burgess, K. (2010) Fluorescent indicators for intracellular pH. *Chem. Rev. 110*, 2709−2728.
(35) Srivastava, J., Barber, D. L., and Jacobson, M. P. (2007) Intracellular pH sensors: design principles and functional significance. *Physiology 22*, 30−39.
(36) Bagur, R., and Hajnóczky, G. (2017) Intracellular Ca2+ Sensing: Its Role in Calcium Homeostasis and Signaling. *Mol. Cell 66*, 780−788.
(37) Czarnik, A. W. (1995) Desperately seeking sensors. *Chem. Biol. 2*, 423−428.
(38) Miyawaki, A., Griesbeck, O., Heim, R., and Tsien, R. Y. (1999) Dynamic and quantitative Ca2+ measurements using improved cameleons. *Proc. Natl. Acad. Sci. U. S. A. 96*, 2135−2140.
(39) Mank, M., Santos, A. F., Direnberger, S., Mrsic-Flogel, T. D., Hofer, S. B., Stein, V., Hendel, T., Reiff, D. F., Levelt, C., Borst, A., et al. (2008) A genetically encoded calcium indicator for chronic in vivo two-photon imaging. *Nat. Methods 5*, 805.
(40) Clapham, D. E. (2007) Calcium signaling. *Cell 131*, 1047−1058.
(41) Pires, D. E. V., Ascher, D. B., and Blundell, T. L. (2014) DUET: a server for predicting effects of mutations on protein stability using an integrated computational approach. *Nucleic Acids Res. 42*, W314−W319.
(42) Jurrus, E., Engel, D., Star, K., Monson, K., Brandi, J., Felberg, L. E., Brookes, D. H., Wilson, L., Chen, J., Liles, K., Chun, M., Li, P., Gohara, D. W., Dolinsky, T., Konecny, R., Koes, D. R., Nielsen, J. E., Head-Gordon, T., Geng, W., Krasny, R., Wei, G.-W., Holst, M. J., McCammon, J. A., and Baker, N. A. (2018) Improvements to the APBS biomolecular solvation software suite. *Protein Sci. 27*, 112−128.
(43) Van Der Spoel, D., Lindahl, E., Hess, B., Groenhof, G., Mark, A. E., and Berendsen, H. J. C. (2005) GROMACS: Fast, flexible, and free. *J. Comput. Chem. 26*, 1701−1718.
(44) Jorgensen, W. L., Maxwell, D. S., and Tirado-Rives, J. (1996) Development and Testing of the OPLS All-Atom Force Field on Conformational Energetics and Properties of Organic Liquids. *J. Am. Chem. Soc. 118*, 11225−11236.
(45) Abascal, J. L. F., and Vega, C. (2005) A general purpose model for the condensed phases of water: TIP4P/2005. *J. Chem. Phys. 123*, 234505.
(46) Darden, T., York, D., and Pedersen, L. (1993) Particle mesh Ewald: An N·log(N) method for Ewald sums in large systems. *J. Chem. Phys. 98*, 10089−10092.
(47) Hess, B., Bekker, H., Berendsen, H. J. C., and Fraaije, J. G. E. M. (1997) LINCS: A linear constraint solver for molecular simulations. *J. Comput. Chem. 18*, 1463−1472.
(48) Bussi, G., Donadio, D., and Parrinello, M. (2007) Canonical sampling through velocity rescaling. *J. Chem. Phys. 126*, 014101.
(49) Parrinello, M., and Rahman, A. (1981) Polymorphic transitions in single crystals: A new molecular dynamics method. *J. Appl. Phys. 52*, 7182−7190.

https://dx.doi.org/10.1021/acssynbio.0c00190
ACS Synth. Biol. 2020, 9, 2427−2439